Electronic structure and electron transport properties of amorphous $Ca_{10}Mg_{90-x}Ga_x$ $(0 \leqslant x \leqslant 40)$ alloys

1998 J. Phys.: Condens. Matter 10 10193

(http://iopscience.iop.org/0953-8984/10/45/007)

J. Phys.: Condens. Matter **10** (1998) 10193–10206. Printed in the UK PII: S0953-8984(98)95441-8

Electronic structure and electron transport properties of amorphous $Ca_{10}Mg_{90-x}Ga_x$ $(0 \leqslant x \leqslant 40)$ alloys

Nobuhiko Takeichi†, Hirokazu Sato‡, Toshiharu Fukunaga†§ and Uichiro Mizutani†

† Department of Crystalline Materials Science, Nagoya University, Furo-cho, Chikusa-ku, Nagoya 464-8603, Japan

‡ Department of Physics, Aichi University of Education, Kariya-shi, Aichi-ken 448-8542, Japan

Received 29 June 1998

Abstract. The resistivity at 300 K of the amorphous $Ca_{10}Mg_{90}$ alloy is only 53 $\mu\Omega$ cm but it increases to 215 $\mu\Omega$ cm when x is increased to 30 in the amorphous $Ca_{10}Mg_{90-x}Ga_x$ alloys. We have studied in this experiment a change in the electronic states immediately below the Fermi level as a function of Ga concentration for amorphous $Ca_{10}Mg_{90-x}Ga_x$ $(0 \leqslant x \leqslant 40)$ alloys by means of photoemission spectroscopy (XPS and UPS), soft x-ray spectroscopy (SXS) and low temperature specific heat measurements. We reveal that the narrow Mg–Ga bonding states are formed below the Fermi level as a result of the hybridization of Mg-3p and Ga-4p states and that this narrow band gives rise to the pseudogap across the Fermi level. Combining the atomic structure data deduced in the preceding paper, we are led to conclude that the Mg_2Ga-like short-range order developed with increasing Ga concentration above $x = 20$ is responsible for causing the narrow p-type bonding states just below the Fermi level and that the simultaneous occurrence of a reduction in the density of states at the Fermi level and an increase in the effective mass results in a sharp increase in resistivity in this system.

1. Introduction

Being stimulated by the first pioneering work by St Amand and Giessen [1], a number of Ca-based amorphous alloys have been synthesized and their atomic and electronic structures have been extensively studied in the past decade [2–10]. From the point of view of the electron transport properties, the amorphous Ca–M binary alloys have received particular attention because the resistivity is only about 50 $\mu\Omega$ cm for M = Mg, whereas it exceeds 400 $\mu\Omega$ cm for M = Al and Ga [3, 4]. Naugle *et al* [5] revealed that the replacement of Al by Ga further increases the resistivity in the Ca–Al–Ga alloys. Mizutani *et al* [6] studied systematically the Al concentration dependence of the electrical resistivity and electronic specific heat coefficient in the amorphous $Ca_{70}Mg_{30-x}Al_x$ and $Ca_{60}Mg_{40-x}Al_x$ ternary alloys and discussed a sharp increase in resistivity with increasing Al concentration in terms of a decreasing density of states at the Fermi level.

Hafner and Jaswal [9, 10] calculated the valence band structure of the amorphous Ca–Mg and Ca–Al alloys in the LMTO method. They pointed out that the Al-3s and Al-3p bands are almost separated, resulting in a deep depression in the density of states at the binding

§ Present address: Research Reactor Institute, Kyoto University, Kumatori-cho, Sennan-gun, Osaka 590-0494, Japan.

0953-8984/98/4510193+14$19.50

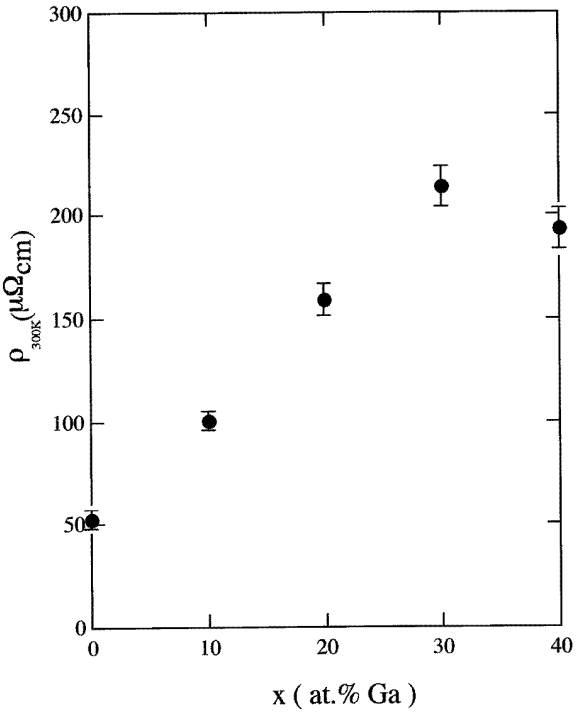

Figure 1. Electrical resistivity at 300 K as a function of Ga concentration in amorphous $Ca_{10}Mg_{90-x}Ga_x$ ($0 \leqslant x \leqslant 40$) alloys.

energy of approximately 3 eV in the amorphous Ca–Al alloys, whereas a continuous free-electron-like band is formed in the amorphous Ca–Mg alloy. They noted the presence of a significant amount of Ca-3d states across the Fermi level and attributed the occurrence of a large resistivity in the amorphous Ca–Al alloys to the presence of the isolated Al-3p states coupled with Ca-3d and Al-3d states at the Fermi level.

Fukunaga *et al* [11] recently revealed that the short-range order associated with Al–Cu and Al–Y atomic pairs affects substantially the electronic states near the Fermi level in the amorphous $Al_x(Cu_{0.4}Y_{0.6})_{100-x}$ ($0 \leqslant x \leqslant 85$) alloys and emphasized that the short-range order plays a critical role in the manifestation of unique electron transport properties. In the preceding paper [12] (hereafter referred to as I), we showed that the Mg_2Ca-type short-range order is present in the amorphous $Ca_{10}Mg_{90}$ alloy but is taken over by the Mg_2Ga-type short-range order with increasing Ga concentration above $x = 20$ in the amorphous $Ca_{10}Mg_{90-x}Ga_x$ alloys. Thus, we consider it to be of great interest to study how the formation of the Mg_2Ga-type short-range order affects the electronic states near the Fermi level and to shed some light on the mechanism for the observed sharp increase in resistivity with increasing Ga concentration in this system. We have studied the Ga concentration dependence of the valence band structure near the Fermi level by means of photoemission spectroscopy, soft x-ray emission spectroscopy and low temperature specific heat measurements for the amorphous $Ca_{10}Mg_{90-x}Ga_x$ ($0 \leqslant x \leqslant 40$) alloys, together with the resistivity and Hall effect measurements. The band calculations were made for the two relevant compounds Mg_2Ca and Mg_2Ga to facilitate the interpretation of the valence band structure of the present amorphous alloys.

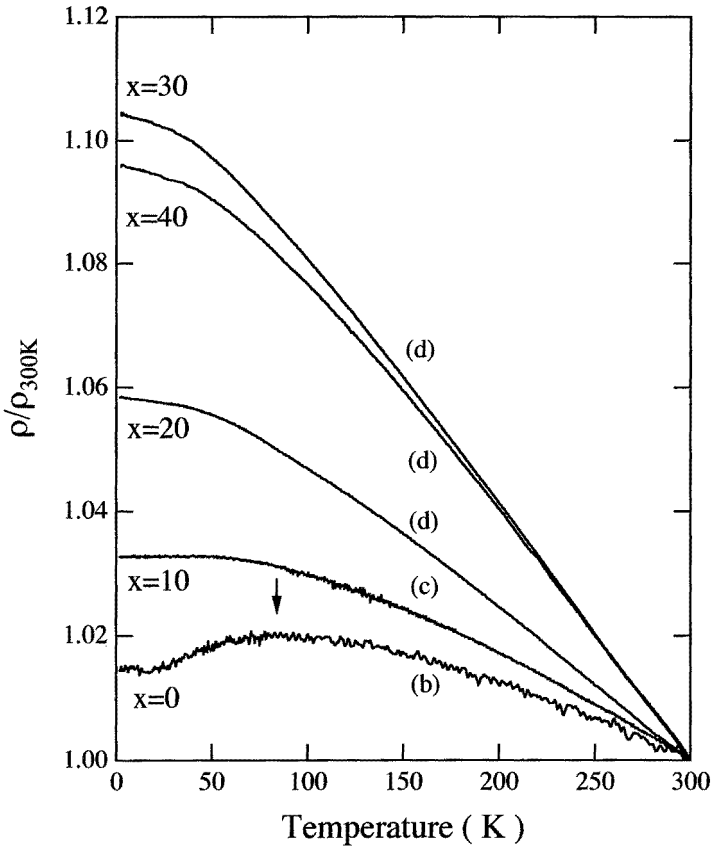

Figure 2. Temperature dependence of resistivity in amorphous $Ca_{10}Mg_{90-x}Ga_x$ ($0 \leqslant x \leqslant 40$) alloys. The resistivity is normalized with respect to the value at 300 K. The arrow indicates the temperature corresponding to the resistivity maximum.

2. Experimental details

The preparation method of the amorphous $Ca_{10}Mg_{90-x}Ga_x$ ($x = 0$, 10, 15, 20, 30, 40) alloys was described in I. For comparison, we have also prepared C12-type Mg_2Ca and Li_2Sb-type Mg_2Ga compounds. The composition of all these samples was checked by electron-probe microanalyser (EPMA) and turned out to agree with the nominal one within $\pm 1\%$. The electrical resistivity was measured in the DC four-terminal method over the temperature range 2–300 K. The Hall coefficient was measured at 300 K using the DC five-terminal method. The low-temperature specific heats were measured in the temperature range 1.5–6 K by the DC adiabatic method. The details are described elsewhere [4, 6, 8].

The photoemission spectra were taken with two different spectrometers. The valence band profiles together with the core levels were measured by using a XPS spectrometer equipped with monochromated Al Kα line (1487 eV) (Surface Science). In addition, the synchrotron radiation (UVSOR, Institute for Molecular Science, Okazaki) with excitation energies in the range 12–20 eV was used to study the excitation energy dependence of the valence band structure near the Fermi level. In all these photoemission measurements, the Fermi level was determined with reference to that of pure Au.

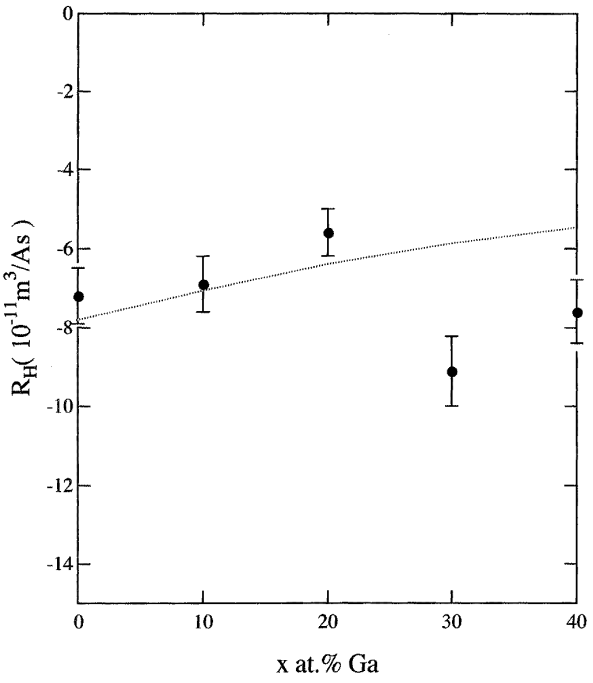

Figure 3. Hall coefficient at 300 K as a function of Ga concentration in amorphous $Ca_{10}Mg_{90-x}Ga_x$ ($0 \leqslant x \leqslant 40$) alloys. A dotted line indicates the free electron behaviour.

Table 1. Electronic properties of amorphous $Ca_{10}Mg_{90-x}Ga_x$ ($0 \leqslant x \leqslant 40$) alloys. The low temperature specific heat data are fitted to equation $C = \gamma T + \alpha T^3$ in the temperature range 1.5–6 K. The Debye temperature Θ_D is calculated from the coefficient α through the relation $\Theta_D = (12\pi^4 R/5\alpha)^{1/3}$, where R is the gas constant.

x	$\rho_{300\ K}$ ($\mu\Omega$ cm)	γ_{exp} (mJ mol^{-1} K^{-2})	Θ_D (K)	$R_H^{300\ K}$ (10^{-11} m^3 A^{-1} s^{-1})
0	53 (±5)	2.17 (±0.08)	301 (±1.2)	−7.2 (±0.7)
10	101 (±5)	2.08 (±0.05)	303 (±0.5)	−6.9 (±0.7)
20	159 (±8)	1.92 (±0.09)	305 (±0.8)	−5.6 (±0.6)
40	214 (±10)	1.74 (±0.15)	302 (±2.1)	−7.6 (±0.8)
40	193 (±10)	2.04 (±0.12)	301 (±2.4)	−7.6 (±0.8)

An electron-probe microanalyser (EPMA-1400, Shimazu) was employed to measure the Mg Kβ soft x-ray emission spectra, which are known to reflect the Mg-3p partial density of states. Its Fermi level was determined by measuring the Mg-2p core level with the XPS spectrometer mentioned above and the Mg Kα line emitted upon the transition from the Mg-2p to Mg-1s states with the soft x-ray spectrometer. The spectra were measured for all amorphous alloys plus the Mg_2Ca and Mg_2Ga compounds.

The band calculations were made for the two compounds Mg_2Ca and Mg_2Ga, both of which crystallize into the hexagonal structure with the unit cell containing 12 and 18 atoms, respectively [13, 14]. The electronic structures are calculated in a self-consistent manner by means of the linear muffin-tin orbital method in the atomic sphere approximation within the

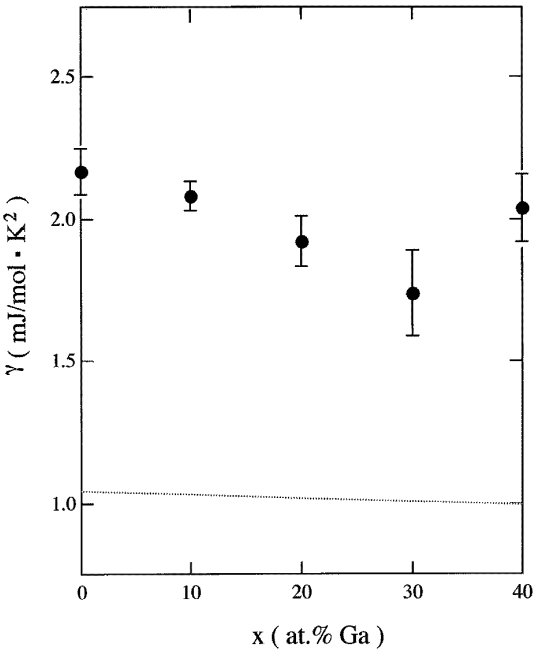

Figure 4. Electronic specific heat coefficient as a function of Ga concentration in amorphous $Ca_{10}Mg_{90-x}Ga_x$ ($0 \leqslant x \leqslant 40$) alloys. A dotted line indicates the free electron behaviour.

local density functional theory [15]. The projected density of states $n_{il}(E)$ for the atomic species i and the azimuthal quantum number l is obtained by k-space integration over the Brillouin zone with the tetrahedron method. The Fermi level is determined by filling 2, 2 and 3 electrons per Mg, Ca and Ga atom into the valence band, respectively.

3. Results and discussion

3.1. Electron transport properties

The resistivity at 300 K for the amorphous $Ca_{10}Mg_{90-x}Ga_x$ ($x = 0$–40) alloys is plotted in figure 1 as a function of Ga concentration. It is clear that the resistivity for the amorphous $Ca_{10}Mg_{90}$ alloy is only 53 $\mu\Omega$ cm but increases sharply up to 215 $\mu\Omega$ cm with increasing Ga concentration. Figure 2 shows the temperature dependence of the resistivity normalized with respect to that at 300 K over the range 1.8–300 K for the present amorphous alloys. The slope of the ρ–T curve is positive in the amorphous $Ca_{10}Mg_{90}$ alloy at low temperatures but slightly negative above about 150 K, resulting in a broad maximum at about 100 K. The temperature corresponding to the resistivity maximum disappears as the Ga concentration is increased. The letters in figure 2, as introduced by Mizutani, refer to the type of ρ–T curve, and were employed to differentiate their characteristic features observed in non-magnetic amorphous alloys and quasicrystals [16]. It has been claimed that the ρ–T types change in the alphabetical sequence with increasing resistivity, regardless of the system chosen. The types (b) to (d) appear successively with increasing resistivity in the amorphous $Ca_{10}Mg_{90-x}Ga_x$ ($x = 0$–40) alloys, lending support to the universal behaviour [16].

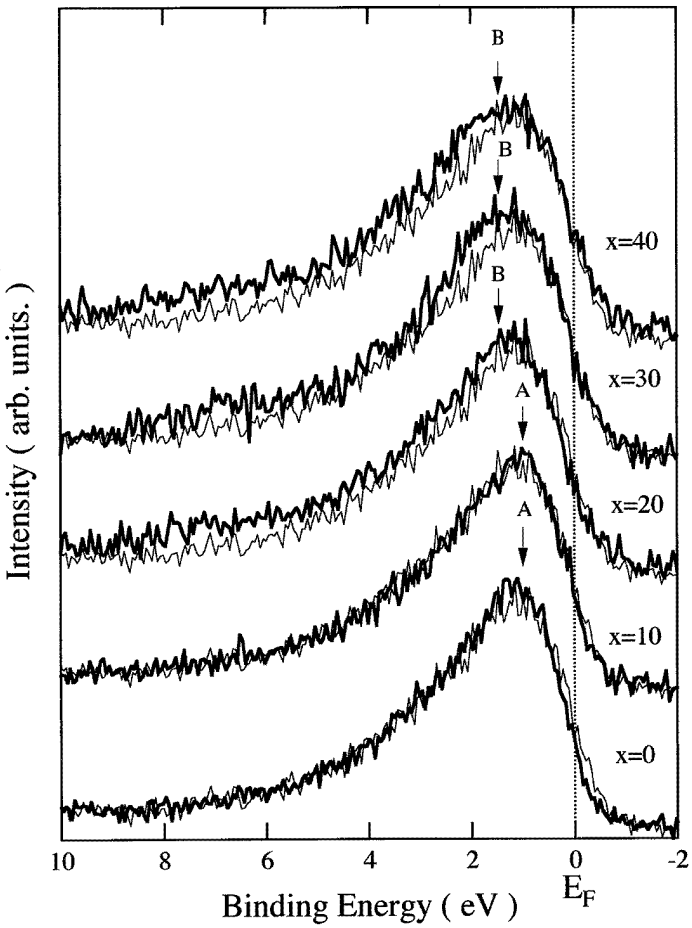

Figure 5. Mg Kβ SXS spectra for amorphous $Ca_{10}Mg_{90-x}Ga_x$ ($0 \leqslant x \leqslant 40$) alloys. Superimposed are the data for pure Mg metal (thin line). Arrows 'A' and 'B' are positioned at binding energies of 1.0 and 1.5 eV, respectively.

Figure 3 shows the Ga concentration dependence of the Hall coefficient at 300 K in the present system. The corresponding free electron Hall coefficient R_H^{free} is calculated in the units of $m^3\ A^{-1}\ s^{-1}$ and drawn in figure 3 as a dashed line by inserting appropriate values into the expression $R_H^{free} = -1.036 \times 10^{-11}(A/d(e/a))$, where A is average atomic weight in g, d is the mass density in g cm^{-3} listed in table 1 in I and e/a is the electron concentration per atom. Here e/a is obtained by assuming that Mg, Ca and Ga donate 2, 2 and 3 electrons per atom, respectively. The Hall coefficient remains negative over the whole concentration range studied and fits well to the free electron value up to $x = 20$. However, the deviation from the free electron model becomes substantial for the amorphous alloys with $x \geqslant 30$.

Numerical data are listed in table 1, together with the low temperature specific heat data discussed below.

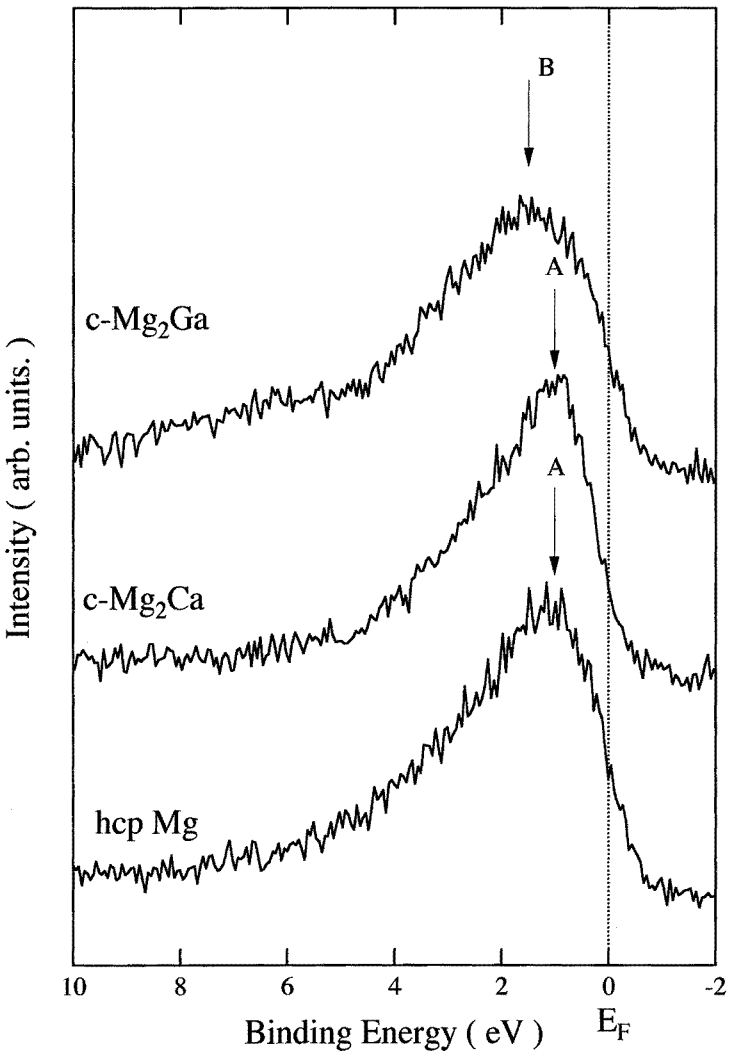

Figure 6. Mg Kβ SXS spectra for pure Mg, Mg_2Ca and Mg_2Ga compounds. Arrows 'A' and 'B' are positioned at binding energies of 1.0 and 1.5 eV, respectively.

3.2. Electronic structure determination

The electronic specific heat coefficient γ_{exp} can be derived from the intercept in the C/T versus T^2 plot for the low temperature specific heat data. Its Ga dependence is shown in figure 4, together with the corresponding free electron value γ_F evaluated in the same manner as the free electron Hall coefficient. In contrast to negligibly small composition dependence of γ_F, the value of γ_{exp} decreases rather sharply up to $x = 30$ with increasing Ga concentration. Hence, we see that the addition of Ga contributes to a decrease in the density of states at the Fermi level and an increase in resistivity in the present alloy system. It may be worthwhile noting that a drop in the resistivity to 200 $\mu\Omega$ cm for the $x = 40$ sample is apparently accompanied by an increase in γ_{exp}.

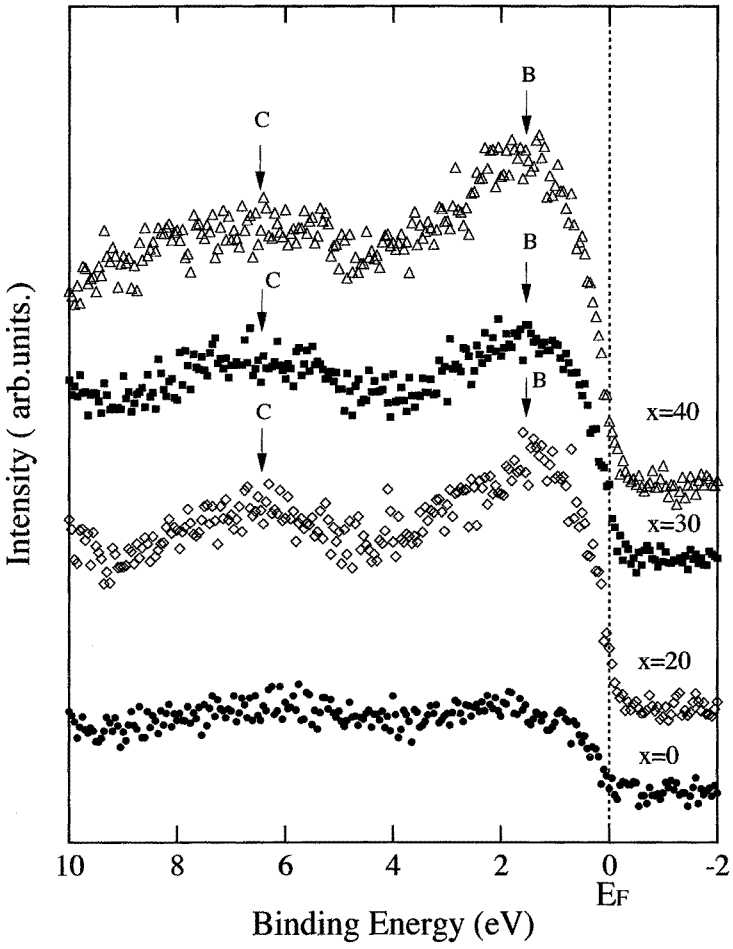

Figure 7. XPS valence band spectra for amorphous $Ca_{10}Mg_{90-x}Ga_x$ ($0 \leqslant x \leqslant 40$) alloys. Arrows 'B' and 'C' are positioned at binding energies of 1.5 and 6.5 eV, respectively.

Another important point to be noted is the fact that the ratio of γ_{exp} over the corresponding free electron value γ_F is fairly large and exceeds two for the amorphous $Ca_{10}Mg_{90}$ alloy. This large enhancement cannot be accounted for solely in terms of the mass enhancement due to the electron–phonon interaction. The contribution due to the two-level tunnelling effect inherent in a disordered system is also too small to account for the large enhancement in the ratio. The Ca-3d states would be certainly non-negligible at the Fermi level and are most likely responsible for this enhancement in spite of its low concentration of only 10 at.%.

Figure 5 shows the Mg Kβ SXS spectra for the amorphous $Ca_{10}Mg_{90-x}Ga_x$ ($x = 0$–40) alloys. This represents the energy spectrum of the soft x-ray radiation emitted upon the transition of the Mg-3p valence electrons into the Mg-1s level and reflects the Mg-3p partial density of states. The spectrum of pure Mg metal is superimposed onto all the spectra of the present amorphous alloys. A difference is scarcely seen between them when the Ga concentration is 0 and 10 at.%. However, the peak for the $x \geqslant 20$ samples is found to shift

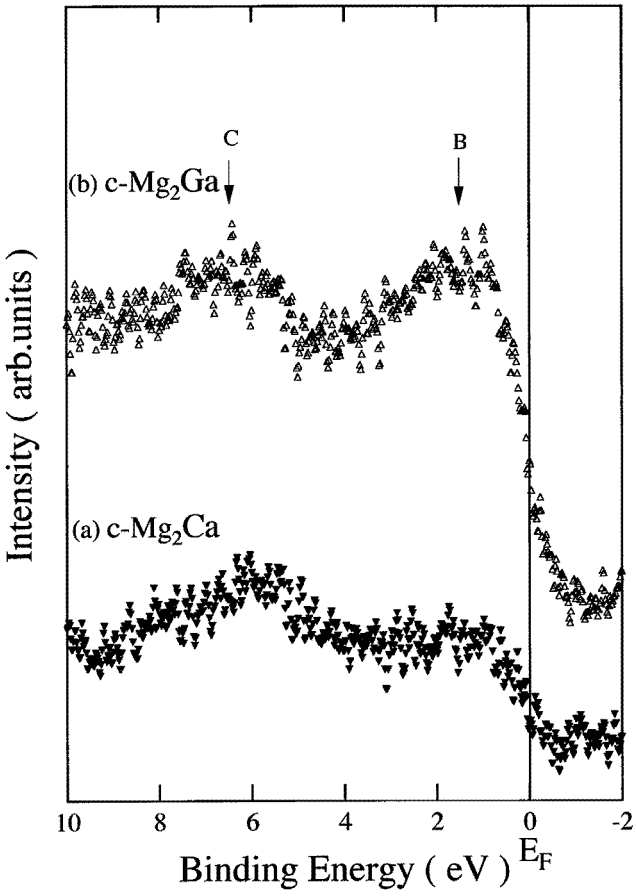

Figure 8. XPS valence band spectra for (a) Mg_2Ca and (b) Mg_2Ga compounds. Arrows 'B' and 'C' are positioned at binding energies of 1.5 and 6.5 eV, respectively.

towards higher binding energies from the position 'A' at 1 eV to 'B' at 1.5 eV, as marked by arrows in figure 5.

The Mg Kβ spectra for the Mg_2Ca and Mg_2Ga compounds are shown in figure 6 in comparison with that of the pure Mg. A good agreement in the spectra can be found between the pure Mg and Mg_2Ca, particularly the main peak, being positioned at 'A' in both cases. Instead, we found that the spectrum of the Mg_2Ga compound having its peak at position 'B' resembles those of the amorphous alloys with $x \geqslant 20$. All these SXS data indicate that the Mg-3p states in the Ga-poor amorphous alloys are well extended as in pure Mg, whereas those in the amorphous alloys with $x \geqslant 20$ resemble more that of the Mg_2Ga compound. Hence, we believe that the peak at 1.5 eV in the Mg Kβ spectrum in the amorphous alloys with $x \geqslant 20$ is most likely caused by the Mg-3p states being perturbed by the Ga-4p states.

In order to extract more information about the role of the Ga atom, we have measured the XPS valence band spectra for a series of the amorphous $Ca_{10}Mg_{90-x}Ga_x$ ($x = 0$–40) alloys. As is clearly seen in figure 7, the XPS spectrum for the amorphous $Ca_{10}Mg_{90}$ alloy is well extended with only a shallow depression at the binding energy of 4 eV. Thus, we

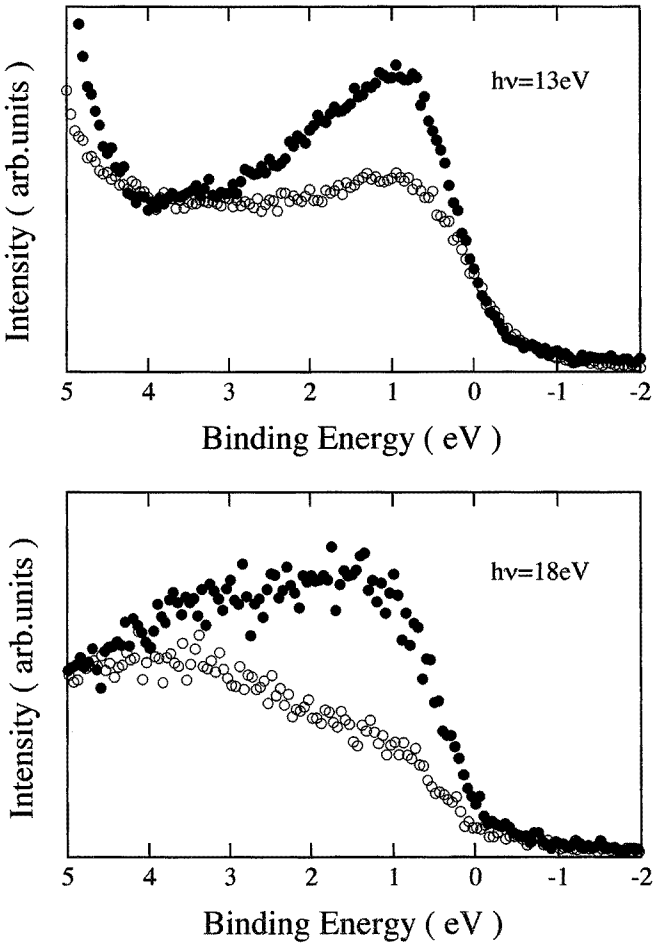

Figure 9. UPS spectra for the amorphous $Ca_{10}Mg_{90}$ (○) and $Ca_{10}Mg_{60}Ga_{30}$ (●) alloys. The spectra were taken with excitation energies of $h\nu = 13$, 16, 18 and 20 eV.

can safely say that the free-electron-like extended states must be responsible for the low resistivity of this amorphous alloy. With increasing Ga concentration, however, the density of states immediately below the Fermi level rapidly grows and results in the peak at the position 'B' of 1.5 eV. In addition, the depression at 4 eV is substantially deepened. The second peak at position 'C' also grows at the binding energy of 7 eV. Here it is important to emphasize that the XPS peak coincides well with peak 'B' at 1.5 eV in the Mg Kβ spectra for the amorphous alloys with $x \geqslant 20$. In I we have concluded that the Mg_2Ga-type short-range order develops above $x = 15$ and becomes more prominent when x exceeds 30. This strongly suggests that the XPS peak grown at 1.5 eV must be related to the formation of the Mg_2Ga-type short-range order.

Figure 8 shows the XPS valence band spectra for the compounds Mg_2Ca and Mg_2Ga. It is clear that the XPS valence band spectrum of the amorphous $Ca_{10}Mg_{90}$ alloy resembles that of the Mg_2Ca compound, whereas the spectra of the amorphous alloys containing more than 20 at.% Ga that of the Mg_2Ga compound. This lends further support to our conclusion

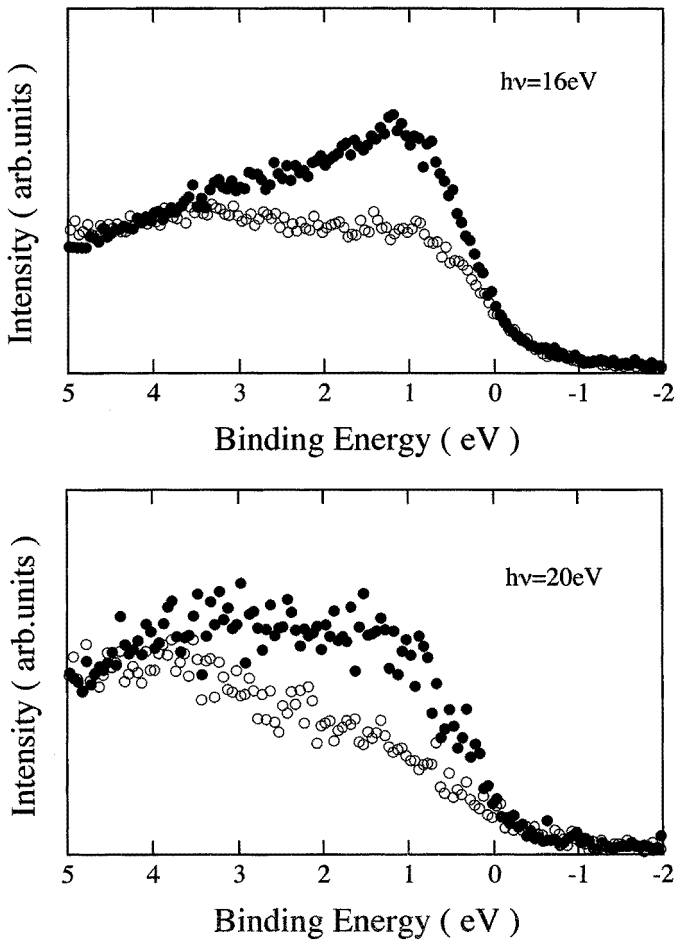

Figure 9. (Continued)

that the narrow XPS peak at 1.5 eV in the amorphous $Ca_{10}Mg_{60}Ga_{30}$ alloy is caused by the bonding states characteristic of the Mg_2Ga compound.

Further detailed information about the bonding states near the Fermi level can be deduced from the excitation energy dependence of the photoemission valence band spectra. This was made possible by using the synchrotron radiation in the ultra-violet energy range 10–20 eV. Two amorphous alloys with $x = 0$ and 30 are chosen as representatives. Figure 9 shows the photoemission spectra with different excitation energies for the two samples. As is clear from the observed spectra, intensities just below the Fermi level are strong when the excitation energy is 13 eV. But intensities immediately below the Fermi level are gradually decreased whereas intensities at higher binding energies around 3–4 eV are increased with increasing the excitation energy in both samples. According to Yeh and Lindau [17], the cross section of the Mg-3p electrons far exceeds that of the Mg-3s electrons in the excitation energies below 13 eV but the situation reverses with increasing excitation energy above 18 eV. This tendency holds for the p and s states of the Ga atom.

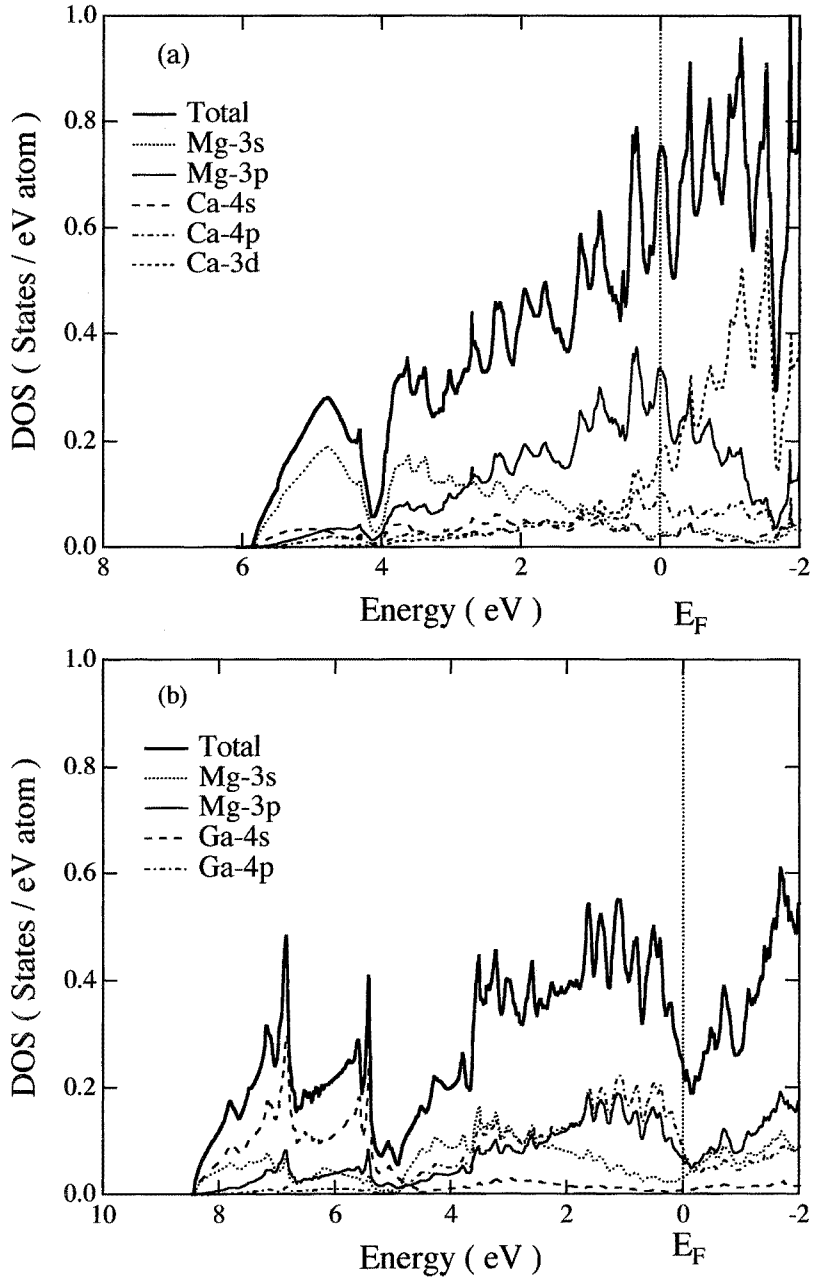

Figure 10. Valence band structures calculated for (a) Mg_2Ca and (b) Mg_2Ga compounds.

The valence band in the amorphous $Ca_{10}Mg_{90}$ alloy must be dominated by Mg-3p and Mg-3s states, since the number of Ca atoms is only 10 at.%. Judging from the excitation energy dependence of the spectra for this binary alloy, we find that its valence band structure is well described by the superposition of the rather well extended Mg-3p and Mg-3s states: the former is centred near the Fermi level whereas the latter is at higher binding energies.

In contrast to the $x = 0$ sample, intensities immediately below the Fermi level are sharply enhanced in the $x = 30$ sample, when the excitation energy is 13 eV. This enhancement can be well accounted for in terms of the formation of the narrow p states comprising the Ga-4p hybridized with Mg-3p states.

In order to strengthen our argument further, we have calculated the density of states for the two compounds Mg_2Ca and Mg_2Ga. As shown in figure 10, the valence band structure of the Mg_2Ca compound is largely composed of the extended Mg-3s and Mg-3p states in good agreement with the observed one for the $x = 0$ sample. In contrast, a deep pseudogap exists across the Fermi level in the Mg_2Ga compound. The pseudogap is apparently formed as a result of the splitting of the hybridized Ga-4p and Mg-3p states into the bonding and antibonding states. At this stage, it may be worthwhile commenting on the peak at the position C observed in the XPS spectra of amorphous alloys with $x \geqslant 20$ in figure 7 and the Mg_2Ga compound in figure 8. A comparison with the band calculations in figure 10(b) suggests the peak arises most likely from the Ga-4s states. However, a similar peak at the binding energy of 6 eV is weakly observed in the $Ca_{10}Mg_{90}$ sample (figure 7) and even more strongly in the Mg_2Ca compound (figure 8), where no Ga-4s states are involved. As far as the Mg_2Ca compound is concerned, the Mg-3s states in figure 10(a) are centred at slightly lower binding energies. Thus, we tend to believe that the rather strong peak at position C observed in the Mg_2Ca compound is due more likely to the O-2p states associated with the unavoidable surface oxidation.

In conclusion, the valence band structure near the Fermi level in the amorphous alloys with $x \geqslant 20$ preserves the feature characteristic of the Mg_2Ga compound, in which the Fermi level falls on the declining slope of the pseudogap. The present experiments confirmed that the narrow bonding peak immediately below the Fermi level is composed of Ga-4p and Mg-3p states. The narrow band grows with increasing Ga concentration, resulting in sharpening the declining slope at the Fermi level. This certainly contributes to an increase in the effective mass of electrons responsible for the electron conduction. In addition, we revealed from the Ga concentration dependence of the electronic specific heat coefficient that the density of states at the Fermi level decreases with increasing Ga concentration. Therefore, a reduction in the number of carriers and an increase in the effective mass occurs concurrently and this explains why the resistivity increases so sharply with increasing Ga concentration in this system.

Acknowledgments

We are grateful to Professor K Soda, Nagoya University and Professor M Kamada, Institute for Molecular Science, for their kind help with the UPS measurements for the present samples. We are also grateful to Professor T Matsuda, Aichi University of Education, for his help with the Hall effect measurements at the early stage of this work.

References

[1] St Amand R and Giessen B C 1978 *Scr. Metall.* **12** 1021
[2] Hong J 1979 *PhD Dissertation* Northeastern University, Boston, MA
[3] Tsai C L, Hong J and Giessen B C 1982 *Proc. 4th Int. Conf. on Rapidly Quenched Metals (Sendai, 1982)* ed T Masumoto and K Suzuki pp 1327–30
[4] Mizutani U and Matsuda T 1983 *J. Phys. F: Met. Phys.* **13** 2115
[5] Naugle D G, Delgado R, Armbruster H, Tsai C L, Callaway T O, Reynolds D and Moruzzi V L 1986 *Phys. Rev.* B **34** 8279
[6] Mizutani U, Sasaura M, Yamada Y and Matsuda T 1987 *J. Phys. F: Met. Phys.* **17** 667

[7] Mizutani U, Sasaura M, Moruzzi V L and Matsuda T 1988 *Mater. Sci. Eng.* **99** 295
[8] Mizutani U, Shimizu T, Fukunaga T, Koyano T, Tanaka K, Yamada M and Matsuda T 1990 *J. Phys.: Condens. Matter* **2** 7825–39
[9] Jaswal S S and Hafner J 1987 *Phys. Rev.* B **38** 7311
[10] Hafner J and Jaswal S S 1987 *Phys. Rev.* B **38** 7320
[11] Fukunaga T, Sugiura H, Takeichi N and Mizutani U 1996 *Phys. Rev.* B **54** 3200
[12] Takeichi N, Fukunaga T and Mizutani U 1998 *J. Phys.: Condens. Matter* **10** 10 179
[13] Nowotny H 1946 *Z. Metallk.* **37** 31
[14] Frank K and Schubert K 1970 *J. Less-Common Met.* **20** 215
[15] Andersen O P 1975 *Phys. Rev.* B **12** 3060
[16] Mizutani U 1993 *Phys. Status Solidi* b **176** 9
[17] Yeh J J and Lindau I 1985 *At. Data Nucl. Data Tables* **32** 1